Energy & Environmental Science

Accepted Manuscript

ROYAL SOCIETY OF CHEMISTRY

www.rsc.org/ees

Journal Name

RSCPublishing

COMMUNICATION

Si-Based Earth Abundant Clathrates for Solar Energy Conversion †

Cite this: DOI: 10.1039/x0xx00000x

Yuping He [a], Fan Sui [b], Susan M. Kauzlarich [c] and Giulia Galli [d]

Received ooth January 2012,
Accepted ooth January 2012

DOI: 10.1039/x0xx00000x

www.rsc.org/

We synthetized a Si-based clathrate, composed entirely of Earth abundant elements, and using ab initio calculations and spectroscopic and Hall mobility measurement, we showed that it is a promising materials for solar energy conversion. We found that the type I clathrate $K_8Al_8Si_{38}$ exhibits a quasi-direct band gap of ≃ 1.0 eV, which may be tuned to span the IR and visible range by strain engineering. We also found that upon light absorption, excited electron and hole states are spatially separated in the material, with low probability of charge recombination. Finally, we computed and measured electron and hole mobilities and obtained values much superior to those of a-Si and approximately 6 to 10 and 10 to 13 time smaller than those of crystalline Si.

The search for Earth abundant materials exhibiting efficient absorption of visible photons is an active area of research, within the fields of photovoltaics[1, 2] and solar to fuel[3, 4] energy conversion. Desirable properties include a direct band gap, low recombination rates and high mobilities of electrons and holes, and stability over a wide temperature range.

We synthesized a new single crystal type I clathrate $K_8Al_8Si_{38}$, and using structural data refined from X-Ray diffraction (XRD) measurements, we generated models for which we computed the electronic and optical properties. Our results showed that this material hold great promises for efficient absorption and photovoltaic conversion of sun light. In particular, our ab initio calculations yielded a quasi-direct band gap of ~1.0 eV for $K_8Al_8Si_{38}$, in agreement with our optical measurements (1.3 eV). The gap is tunable by strain engineering within the IR and visible ranges. In addition we found that excited electrons and holes generated upon absorption are spatially separated on different cages, with mobilities much superior to those of a-Si.

The single crystal type-I clathrate $K_8Al_8Si_{38}$ was synthesized using a simple mixing and baking method. Single crystal X-ray diffraction data showed that $K_8Al_8Si_{38}$ crystallizes in a type I clathrate structure, with $Pm\bar{3}n$ space group, and lattice parameter (a)=10.4802(16) Å (see Table SI of supplementary material and deposited CIF data at C

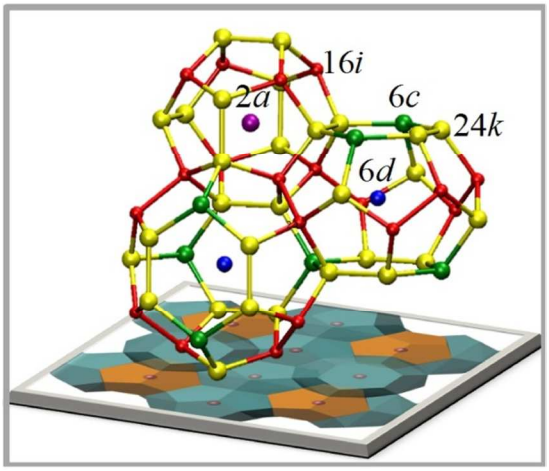

Fig. 1 Ball and stick representation of the type I clathrate investigated in this work : $K_8Al_8Si_{38}$, composed of dodecahedral and tetrakaidecahedral cages. Within the Wyckoff sites representation of the structure, the center of the cages are denoted by 2*a* (purple) and 6*d* (blue) for dodecahedral and tetrakaidecahedral cages, respectively; the host structure is represented by three inequivalent crystallographic sites: 6*c* (green), 16*i* (red) and 24*k* (yellow).

at Cambridge Crystallographic Data Centre : deposition number CCDC 990683). An electron microprobe analysis revealed a 7.63(7):38.35(7) Al to Si ratio, which was kept fixed in our structural refinement. There are three distinct Wyckoff sites in the framework (see Fig.1): 6c, 16i and 24k. Mixed Al/Si occupancies were allowed on all three framework sites; the model with Al on the 6c and 24k sites resulted in the best fit, and yielded the 6c and 24k sites as being 79% and 12.1% occupied by Al, respectively. This result is consistent with those of previous studies showing that Al atoms preferentially occupy 6c sites in $Ba_8Al_xSi_{46-x}$[5]. The occupancies at guest atoms sites, 2a and 6d, by K and 16i site by Si were also examined in the refinement. No vacancy was found, and therefore in the final refinement those sites were assumed to be occupied. Our fit to XRD data indicated that the K atoms at 2a sites exhibits large anisotropic thermal displacements. However a site split model was eventually not adopted as it failed to improve the refinement procedure. Additional detail about site occupancies are

Table 1 Direct (d) and indirect (i) electronic band gaps (eV) calculated by using Density Functional Theory and the PBE functional (first and second columns) for six $K_8Al_8Si_{38}$ samples : A, B, C with 5*c*2*k*1*i* configuration and D,E,F with 6*c*2*i* configuration for different Al occupancy sites (see text). The fourth column reports gaps calculated using many body perturbation theory within the G_0W_0 approximation, for optimized geometries at zero pressure and temperature. The fifth and sixth columns show values of gaps evaluated for tensile and compressive strains corresponding to a pressure of 5.8 GPa. Figures in italics were estimated based on the G_0W_0 correction obtained for sample A and D (see text).

Sample	$E_g^{PBE}(i)$	$E_g^{PBE}(d)$	$E_g^{GW}(d)$	$E_g^{PBE}(d)$ @ −5.8*GPa*	$E_g^{PBE}(d)$ @ 5.8*GPa*
A	0.56	0.56	0.81	0.69	0.43
B	0.67	0.73	*1.06*	*0.90*	*0.56*
C	0.73	0.79	*1.15*	*0.97*	*0.61*
D	0.56	0.69	*1.00*	0.85	0.53
E	0.40	0.44	*0.64*	*0.54*	*0.34*
F	0.60	0.74	*1.07*	*0.91*	*0.57*

provided in Table SII.

We generated six snapshots of the $K_8Al_8Si_{38}$ structure using the guidelines for site occupancy proposed by Christensen et al[6]. These are 6c2i, 5c2k1i, 8k, 3c5i, 3c5k and 8i, where the letters denote atomic sites, and the digits denote the number of sites occupied by Al atoms. We then computed the total energies of the six samples using first principles density functional theory calculations within the Perdew-Burke-Ernerhof (PBE) approximation[7, 8], and we identified the two most stable configurations: 6c2i and 5c2k1i. These turned out to be consistent with those recently observed experimentally in the type I clathrate $Ba_8Al_xSi_{46-x}$[5] and, most importantly, with those found in the single crystal $K_8Al_8Si_{38}$ grown in our experiments. The comparison of site distances from single crystal refinements and theoretical calculations is given in Table SIII. We found that not only the value of site distances but also the relative order of distances obtained by first principle optimizations is in satisfactory agreement with experimental results, indicating that the models generated in our calculations are adequate to represent the structure of type I clathrate obtained in experiments. The lattice constant of the optimized model is 10.578 Å. i.e. 0.9% larger than the measured value (10.4802 Å).

Having identified the most stable sets of configurations of $K_8Al_8Si_{38}$, we computed the band structures (Fig. 2) of several of those, with Al substituted at different sites, in order to mimic the range of atomic substitutions possibly existing in the real material. We considered three 5*c*2*k*1*i* (A,B,C) and three 6*c*2*i* (D,E,F) samples. Most calculations were conducted at the DFT level and one sample (A) was carefully analyzed using many body perturbation theory (MBPT) at the G_0W_0 level [9] (see Fig. S1). Our DFT band structure calculations are consistent with those reported in Ref [10], where a thermoelectric study of type I clathrates was reported, although our computed gaps differ. We found that the position of Al in the Si cages may significantly influence the valence bands position, while the conduction bands are largely unaffected (see Fig. 2a and 2b). Fig. 2c shows the G_0W_0 corrected band structure of sample A with respect to that obtained at the DFT-PBE level. We found a rigid shift

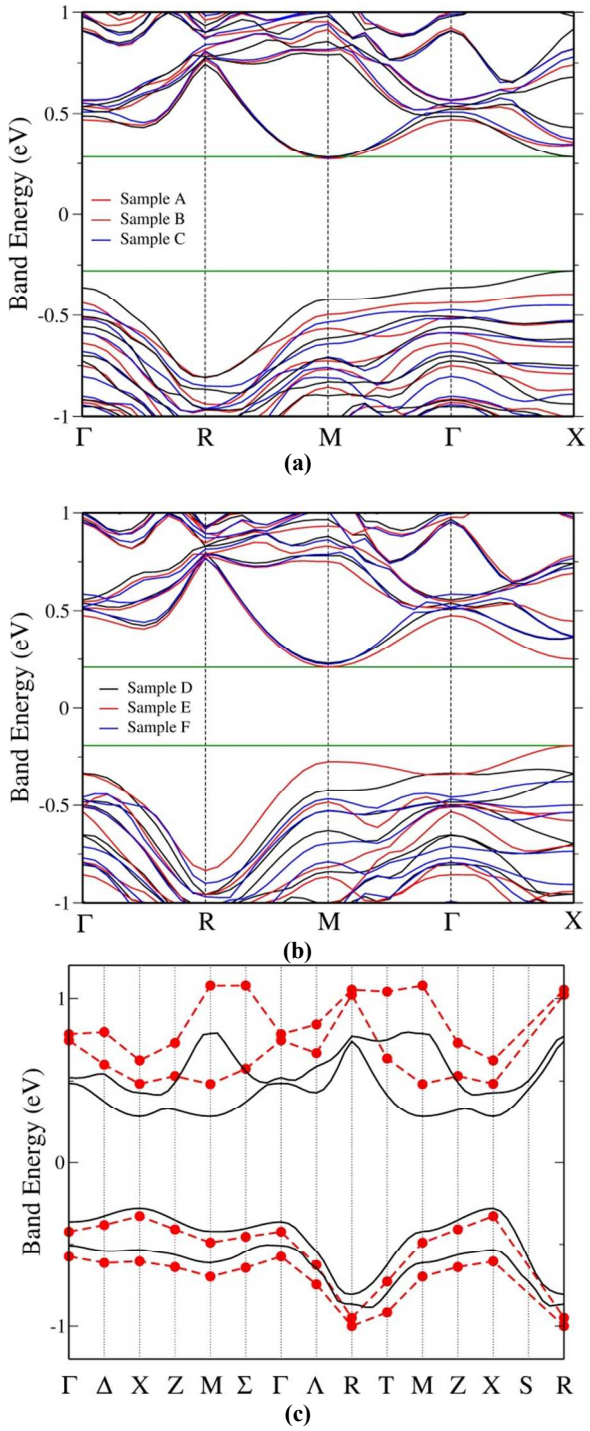

Fig. 2 (a) Band structure of $K_8Al_8Si_{38}$ with Al on five 6c sites, two 24k sites and one 16i sites (5c2k1i configurations), for samples A (black), B (red) and C (blue), calculated using DFT-PBE. (b) Band structure of $K_8Al_8Si_{38}$ with Al on six 6c sites, two 16i sites (6c2i configurations) for samples D (black), E(red) and F(blue), calculated using DFT-PBE. (c) Band structure of $K_8Al_8Si_{38}$ (sample A) calculated using DFT-PBE (black) and many body perturbation theory within the G_0W_0 approximation (red), respectively.

of the uppermost valence band (VB) to lower energy (0.04 eV), and of the lowest conduction band (CB) to higher energy (0.21 eV), yielding a band gap (0.81 eV) increase of approximately 45 % with respect to that computed within DFT-PBE (0.56 eV). We then

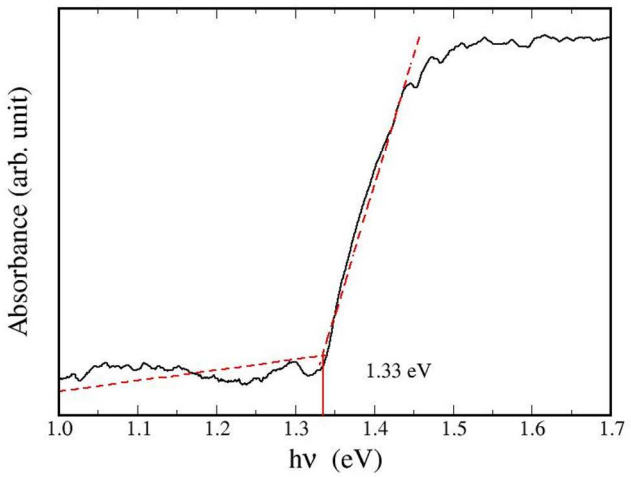

Fig. 3 The measured absorbance as a function of photon energy using a UV-Vis spectrophotometer. The combined (i.e. direct and indirect) band gap value (1.33 eV) is indicated by the intersection of the fitted base line and the absorption edge (red dash lines).

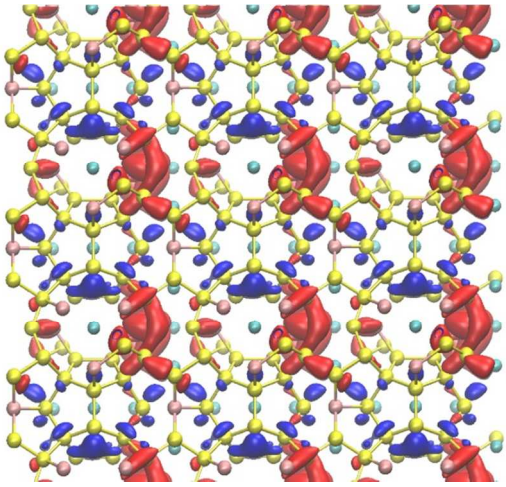

Fig. 4 Isosurfaces of the square moduli of the valence band maximum (red) and conduction band minimum (blue) single particle states of type I clathrate $K_8Al_8Si_{38}$; yellow, pink and cyan spheres represent Si, Al and K atoms, respectively.

assumed that a similar increase would approximately apply to all other samples, in going from the DFT/PBE to the G_0W_0 levels of theory (All samples have similar geometries and exhibit the same kind of bonds). The computed gaps varies between 0.44 and 0.79 eV within PBE and between 0.64 and 1.15 eV within G_0W_0 at normal conditions. Irrespective of the sample and the level of theory, we found that all of our models have direct or quasi-direct band gaps, with differences between direct and indirect gaps of at most ≃ 0.14 eV. Specifically, taking into account thermal energy effects ($k_BT \sim 0.03eV$ at 300 K), we identified four samples (A, B, C and E) with direct band gaps (see Table I).

We estimated the exciton binding energy (E_b) of the material for sample A from the formula $E_b = e^2/(\varepsilon a_0^*)$ [11], where the dielectric constant ε was computed using density functional perturbation theory[12, 13] and $a_0^* = m_e \varepsilon a_0 / m^*$; here a_0 is the Bohr radius, m_e the electron mass, m^* the effective reduced mass, obtained from the computed effective mass (see below). We obtained ε ~12.86, a value similar to that of c-Si (12.81 at the same level of theory), and a_0^*~16 Å, which is about 3 times smaller than in c-Si (~ 42 Å) [10]. Hence our estimate for the exciton binding energy is approximately 0.06 eV. Therefore we expect that the trends found for the quasi-particle gaps reported in Table I are unaffected in the case of optical gaps, which are obtained by subtracting exciton binding energies from the electronic gaps.

Next we analyzed the variation of the gaps caused by possible strain fields present in the material due, e.g. to growth conditions. We computed the electronic properties of $K_8Al_8Si_{38}$ samples A and D under compressive and tensile strain, corresponding to P = +5.8 GPa and -5.8 GPa (the former value of P is obtained when considering the experimental lattice constant). We found a decrease (increase) of about 23 % in the gap under compression (tensile strain), with no notable change in the shape of the bands and hence no modification of the nature of the gaps that remained (quasi)-direct. Hence we conclude that the computed band gap within G_0W_0 under the effect of strain are between 0.5 and 1.4 eV. These band gaps fall mostly in the energy range of 1~1.5 eV, which yields the maximum photon absorption from solar radiation[14]. These results suggest that one may tune the optical absorption of the material in a range between IR and visible by strain engineering, with great advantage with respect to materials that absorb just in a narrow energy window, and improved efficiency for solar energy conversion.

We measured the band gaps by transmission. Fig. 3 shows the measured absorbance as a function of photon energy obtained by using a Perkin-Elmer Model Lambda 750 UV/Vis/NIR spectrophotometer; the measured band gap is ~1.33 eV (see Supplementary for the details of measurement). To estimate the direct and indirect band gap, we converted the absorbance to the Kubelka-Munk function F(R), and using a Tauc plot we obtained a direct band gap of 1.29 eV and an indirect band gap of 1.06 eV (see Fig. S5 and S6), in excellent agreement with our theoretically predicted values of ~1.0 eV with at most a 0.14 eV difference between direct and indirect band gaps.

In addition to strain, it is reasonable to expect the presence of defects, e.g. vacancies and unbalanced stoichiometric ratios in some of the experimental samples. We generated samples with vacancies by removing one silicon atom from the unit cell of each of the $K_8Al_8Si_{38}$ configurations (A,B,C,D and E) shown in Table I (this corresponds to ~$1x10^{19}$ cm^{-3} density of defects in the material). In samples A, B and C a Si atom was removed from the 6c site; the resulting vacancy had only one Al neighbour in A and B (on the 16i and 6c site, respectively), but two Al neighbours in C (one on 6c and the other one on 16i); in samples D and E a Si atom was removed from 16i and 24k sites, respectively and the resulting vacancy had no Al neighbours. The computed total energies showed that the defective B and C samples, with Si missing from a 6c sites, are the most stable ones (see Table SIV) with respect to other samples (A, D and E) and, importantly, they are both semiconducting, with PBE band gaps of 0.52 eV and 0.48 eV. Samples A, D and E were instead found to be metallic (see Table SIV). These results indicate that the presence of possible vacancies in $K_8Al_8Si_{38}$ is not likely to change its semiconducting properties and the nature of its gap.

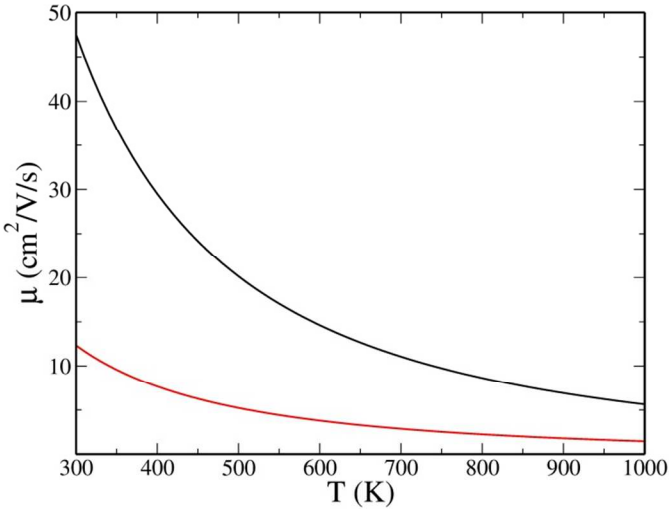

Fig. 5 Calculated carrier mobilities (electrons, black curve, and holes, red curves) of type I clathrate $K_8Al_8Si_{38}$ as a function of temperature (T) with carrier concentration $1x10^{18}$ cm^{-3}, using the single Kane band model (see text).

To explore the effect of unbalanced stoichiometry on the band gaps, we created four samples starting from configuration A: $K_6Al_8Si_{38}$, $K_8Al_6Si_{40}$, $K_7Al_7Si_{39}$, and $K_6Al_6Si_{40}$. We found that $K_6Al_8Si_{38}$ is a p-type semiconductor with Fermi energy slightly overlapping with the valence bands (i.e. 0.18 eV below the valence band maximum); instead $K_8Al_6Si_{40}$ is a n-type semiconductor with the Fermi energy slightly over-lapping with the conduction bands (i.e. 0.19 eV above the conduction band minimum). $K_7Al_7Si_{39}$ and $K_6Al_6Si_{40}$ are intrinsic semiconductors with band gaps of 0.70 eV and 0.80 eV, respectively. Therefore for the family of type I clathrates K_X Al_Y Si_{46-Y}, we found that if the condition X+Y+4x(46-Y)=184 is satisfied (i.e. a zintl phase is realized), the system is a semiconductor. By decreasing the number of K and Al atoms, one may increase the band gap: for example, the band gap of $K_7Al_7Si_{38}$ is 0.70 eV and that of $K_6Al_6Si_{38}$ is 0.80 eV, to be compared with that of sample A, 0.56 eV. We note that the calculated band gap of Si_{46} is 1.33 eV at the DFT/PBE level.

In addition to efficient absorption, key properties of materials for photovoltaic applications are the spatial localization of electrons and holes and their mobilities. Fig. 4 shows the calculated square moduli of the top valence band wavefunction (VBM, red) and bottom conduction band wavefunction (CBM, blue) of sample A (Table I). Interestingly, we found that the VBM is localized in the large cages around the Al atoms, while the CBM is localized on the small cages around the Si atoms, with very limited spatial overlap between the two, indicating a low probability of charge recombination. This conclusion holds for any of the structures of $K_8Al_8Si_{38}$ examined in this work, although the spatial localizations of VBM and CBM depend on the positions of Al and Si atoms (see Fig. S2).

Finally we computed the carrier mobilites of electrons and holes as a function of concentration and temperature (*T*) for sample A by using the single band Kane model[15], where all parameters were derived from first principles:

$$\mu = \frac{2\pi\hbar^4 eB}{m_I^*(2m_b^* k_B T)^{3/2}\Xi^2}\frac{3^0F_{-2}^1}{^0F_0^{3/2}}$$

$$^nF_l^m = \int_0^\infty (-\frac{\partial f}{\partial \zeta})\zeta^n(\zeta+\alpha\zeta^2)^m[(1+2\alpha\zeta)^2+2]^{l/2}d\zeta$$

where $\hbar$ is the Planck constant, *e* the electronic elementary charge, k_B the Boltzmann constant, ζ the reduced carrier energy (ζ/k_BT) and $\alpha=k_BT/E_g$, where E_g is the electronic gap; $f=1/(e^{\zeta-u}+1)$ is the Fermi-Dirac distribution, and u the Fermi energy. The effective mass $m_I^* = 3(2/m_\perp^* + 1/m_\parallel^*)^{-1}$ and $m_b^* = (m_\perp^{*2}m_\parallel^*)^{1/3}$ were determined by computing $m_\perp^*$ and $m_\parallel^*$ from quadratic fits of the bands at X and M for the electrons, and at X for the holes (see Fig. S3). We found that both $m_\perp^*$ and $m_\parallel^*$ at X are similar to those at M, and $m_I^*=m_b^*$ =0.68 m_e for electrons and $m_I^*=m_b^*$=1.03 m_e for holes. The bulk modulus B was computed using the Newton-Laplace formula: $B=v_s\rho$ where ρ is the density and v_s the speed of sound. The latter was obtained by averaging the group velocities of longitudinal ($v_{g,l}$) and transverse ($v_{g,t}$) modes ($v_s=(v_{g,l}+v_{g,t1}+v_{g,t2})/3$) as computed by linear fits, close to the Γ point, of the phonon dispersion curves calculated using density functional perturbation theory[12, 13, 16]. The computed bulk modulus is $2.1x10^{10}$ Pa, substantially smaller than that of crystalline Si ($9.7x10^{10}$ Pa). The electron-phonon and hole-phonon coupling energies were calculated from the deformation potential[17-19]: $\Xi = V_0(\Delta E_{CBM}/\Delta V)$ and $\Xi = V_0(\Delta E_{VBM}/\Delta V)$, where V_0 is the equilibrium volume of the crystal, ΔV is the volume change, ΔE_{CBM} the change of the energy of the conduction band minimum, and ΔE_{VBM} that of the valence band maximum. We obtained Ξ=7.55 eV and Ξ=8.67 eV for electrons and holes, respectively (to be compared, e.g. to those of Si: 10.57 eV (electrons) and 5.39 eV (holes) [20]). We first calculated carrier (electron and hole) mobilities as a function of carrier concentrations at 300 K and extrapolated to the intrinsic carrier concentration (n) limit of $1x10^{18}$ cm^{-3} (see Fig. S4). Using such value, we then computed the carrier mobilities as a function of temperature shown in Fig.5. The computed electron mobility of $K_8Al_8Si_{38}$ is ~49 $cm^2/V/s$ at room temperature; we measured the electron mobility by Hall effect and we obtained a value of ~39 $cm^2/V/s$ (see Supplementary Information) in good agreement with our theoretical predictions.

We found that the electron and hole mobilities of the type I clathrate $K_8Al_8Si_{38}$ are smaller than those of diamond Si[20-22] by a factor of six to ten at room temperature. The lower values of the mobilities are partly due to the slight amount of disorder present in the cages. However the computed values of μ are better than those of SnS[23], and comparable to those of Cu_2O[24], which are promising semiconductors for photovoltaic applications. Importantly we found that the μ of $K_8Al_8Si_{38}$ is much superior to those of, e.g. a-Si: 1 $cm^2/V/s$ for electrons and 0.01 $cm^2/V/s$ for holes[25-28] and to those of organic materials: ~ 0.008 $cm^2/V/s$ for electrons and ~ 0.002 for holes[29]. In addition, the ratio μ_e/μ_h is ~ 5 in $K_8Al_8Si_{38}$, while it can be as high as 100 in a-Si (it is ~ 3 in c-Si). Finally we note that a thermal analysis using differential scanning calorimetry (DSC) showed that $K_8Al_8Si_{38}$ is stable up to 1270 K[30].

Conclusions

We synthetized a new type I clathrate composed entirely of Earth abundant elements, $K_8Al_8Si_{38}$, and we showed that it is a promising material for solar energy conversion, with a quasi direct band gap of ~ 1 eV, relatively high mobilities and excited electron and hole states spatially separated, with low probability of charge carrier recombination. The computed and measured values of the band gap and electron mobilities showed very good agreement.

Acknowledgments

We thank Ding Pan and Márton Vörös for useful discussions. YH and GG would like to acknowledge the use of the computational facilities at NERSC at LBNL, and funding from DOE/BES grant No. DE-FG02-06ER46262. FS and SK would like to acknowledge NSF grant DMR-1100313.

Notes and references

[a] *Department of Chemistry, University of California, One Shields Avenue Davis, CA 95616, USA. Fax: 530-752-3172 Tel: 530-752-0906 E-mail: yphe@ucdavis.edu*

[b] *Department of Chemistry, University of California, One Shields Avenue Davis, CA 95616, USA. Fax: 530-752-8995 Tel: 530-752-4756 E-mail: fsui@ucdavis.edu*

[c] *Department of Chemistry, University of California, One Shields Avenue Davis, CA 95616, USA. Fax: 530-752-8995 Tel: 530-752-4756 E-mail: smkauzlarich@ucdavis.edu*

[d] *Institute for molecular engineering, The University of Chicago, 5747 South Ellis Avenue; Jones Laboratory 215, Chicago, IL 60637, USA. Fax: 530-752-3172 ; Tel: 530-754-9554 ; E-mail: gagalli@uchicago.edu*

† Electronic Supplementary Information (ESI) available: The details of sample synthesis, X-ray diffraction analysis and the measurement of band gap and Hall moblity. The additional theoretical results, i.e. vacancies comparison, convergence in G_0W_0 calculations, effective mass calculations and the mobilities as a function of carrier concentrations. See DOI: 10.1039/b000000x/

1. L. El Chaar, L. A. lamont and N. El Zein, *Renewable and Sustainable Energy Reviews*, 2011, **15**, 2165-2175.
2. T. M. Razykov, C. S. Ferekides, D. Morel, E. Stefanakos, H. S. Ullal and H. M. Upadhyaya, *Solar Energy*, 2011, **85**, 1580-1608.
3. F. E. Osterloh, *Chemical Society Reviews*, 2013, **42**, 2294-2320.
4. M. G. Walter, E. L. Warren, J. R. McKone, S. W. Boettcher, Q. Mi, E. A. Santori and N. S. Lewis, *Chemical Reviews*, 2010, **110**, 6446-6473.
5. J. H. Roudebush, C. de la Cruz, B. C. Chakoumakos and S. M. Kauzlarich, *Inorganic chemistry*, 2011, **51**, 1805-1812.
6. M. Christensen, S. Johnsen and B. B. Iversen, *Dalton Transactions*, 2010, **39**, 978-992.
7. J. P. Perdew, K. Burke and M. Ernzerhof, *Physical Review Letters*, 1996, **77**, 3865-3868.
8. J. P. Perdew, K. Burke and M. Ernzerhof, *Physical Review Letters*, 1997, **78**, 1396-1396.
9. A. Marini, C. Hogan, M. Grüning and D. Varsano, *Computer Physics Communications*, 2009, **180**, 1392-1403.
10. K. Nakamura, S. Yamada and T. Ohnuma, *Materials Transactions*, 2013, **54**, 276-285.
11. M. Dvorak, S.-H. Wei and Z. Wu, *Physical Review Letters*, 2013, **110**, 016402.
12. P. Giannozzi, S. de Gironcoli, P. Pavone and S. Baroni, *Physical Review B*, 1991, **43**, 7231-7242.
13. S. Baroni, S. de Gironcoli, A. Dal Corso and P. Giannozzi, *Reviews of Modern Physics*, 2001, **73**, 515-562.
14. F. Meillaud, A. Shah, C. Droz, E. Vallat-Sauvain and C. Miazza, *Solar Energy Materials and Solar Cells*, 2006, **90**, 2952-2959.
15. H. Wang, Y. Pei, A. D. LaLonde and G. J. Snyder, *Proceedings of the National Academy of Sciences*, 2012, **109**, 9705-9709.
16. Y. He and G. Galli, *submitted*, 2014.
17. J. Bardeen and W. Shockley, *Physical Review*, 1950, **80**, 72-80.
18. S. Bruzzone and G. Fiori, *Applied Physics Letters*, 2011, **99**, -.
19. C. G. Van de Walle, *Physical Review B*, 1989, **39**, 1871-1883.
20. M. V. Fischetti and S. E. Laux, *Journal of Applied Physics*, 1996, **80**, 2234-2252.
21. N. D. Arora, J. R. Hauser and D. J. Roulston, *Electron Devices, IEEE Transactions on*, 1982, **29**, 292-295.
22. F. Schindler, M. C. Schubert, A. Kimmerle, J. Broisch, S. Rein, W. Kwapil and W. Warta, *Solar Energy Materials and Solar Cells*, 2012, **106**, 31-36.
23. P. Sinsermsuksakul, Heo, J., Noh, W., Hock, A. S. and Gordon, R. G., *Adv. Energy Mater.*, 2011, **1**.
24. Y. S. Lee, M. T. Winkler, S. C. Siah, R. Brandt and T. Buonassisi, *Applied Physics Letters*, 2011, **98**, -.
25. T. Tiedje, B. Abeles, D. L. Morel, T. D. Moustakas and C. R. Wronski, *Applied Physics Letters*, 1980, **36**, 695-697.
26. M. Hoheisel and W. Fuhs, *Philosophical Magazine Part B*, 1988, **57**, 411-419.
27. E. A. Schiff, *Journal of Non-Crystalline Solids*, 2006, **352**, 1087-1092.
28. A. R. Moore, *Applied Physics Letters*, 1977, **31**, 762-764.
29. Y. Zhang, S.-C. Chien, K.-S. Chen, H.-L. Yip, Y. Sun, J. A. Davies, F.-C. Chen and A. K. Y. Jen, *Chemical Communications*, 2011, **47**, 11026-11028.
30. , About 20 mg K8Al8Si38 powder was used for Thermogravimetry and differential Scanning Calorimetry (TG-DSC) analysis. Thermal behaviour was tested from room temperature to 1270K. No significant melting or phase transition processes can be identified in this temperature range.

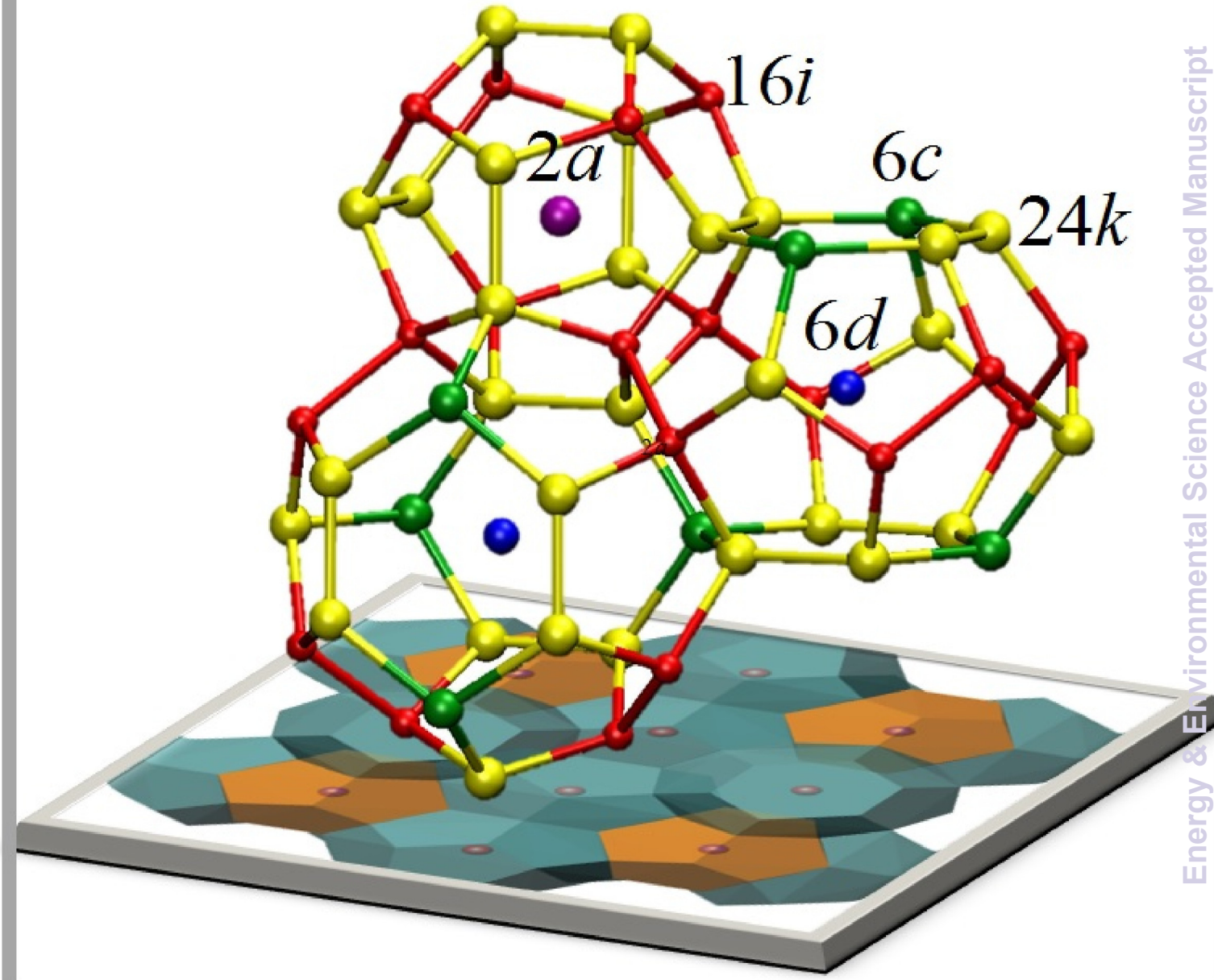

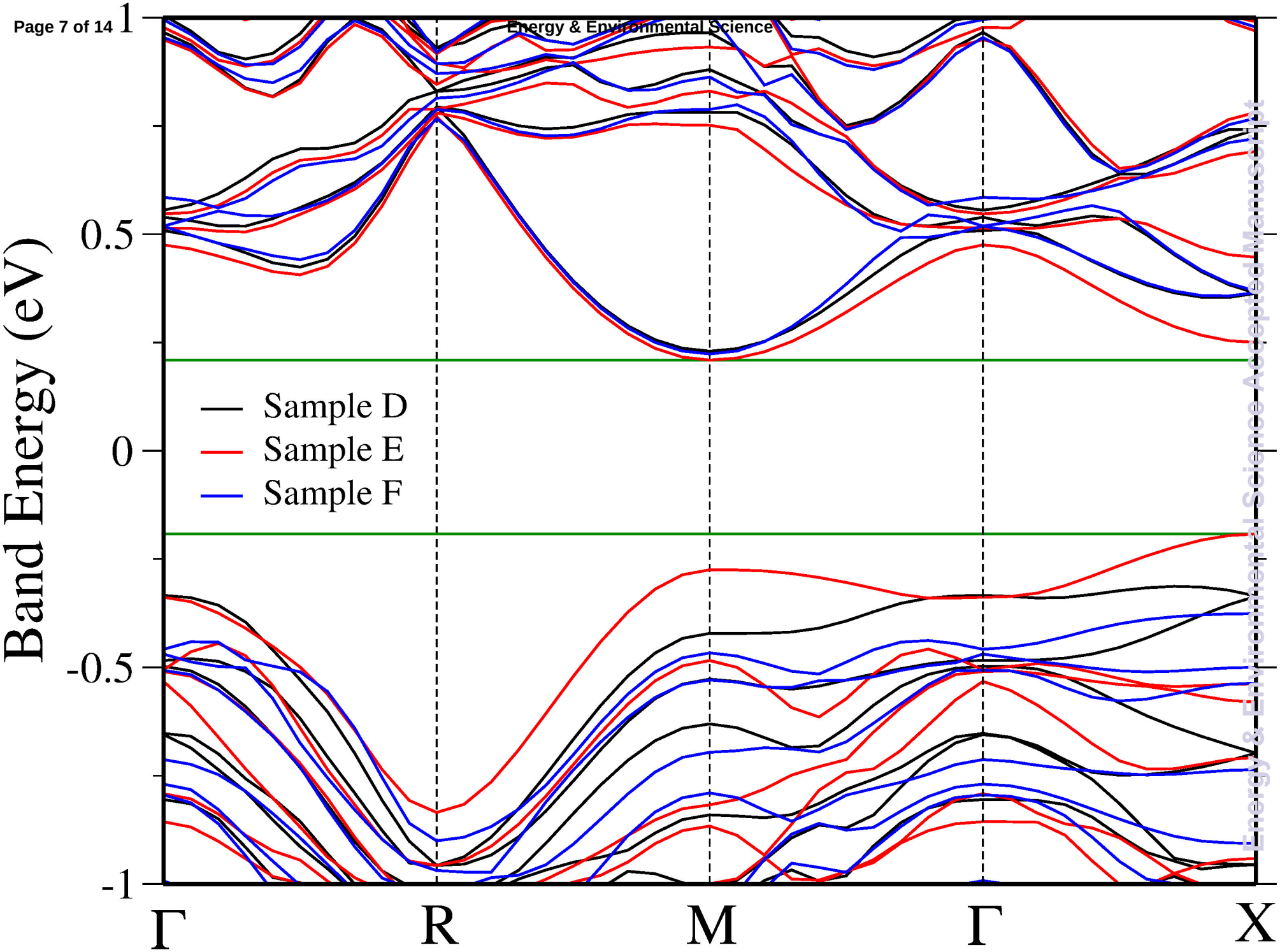

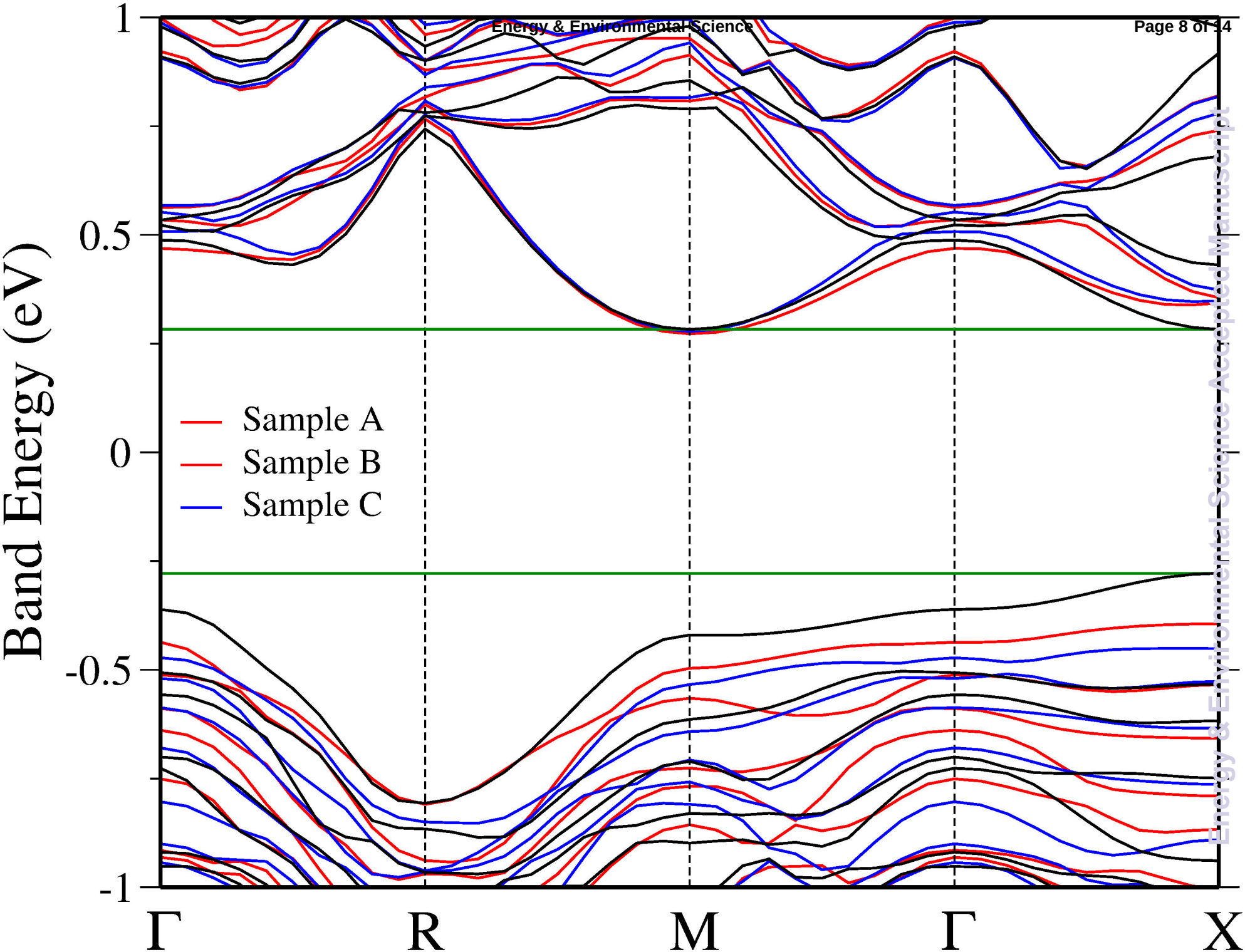

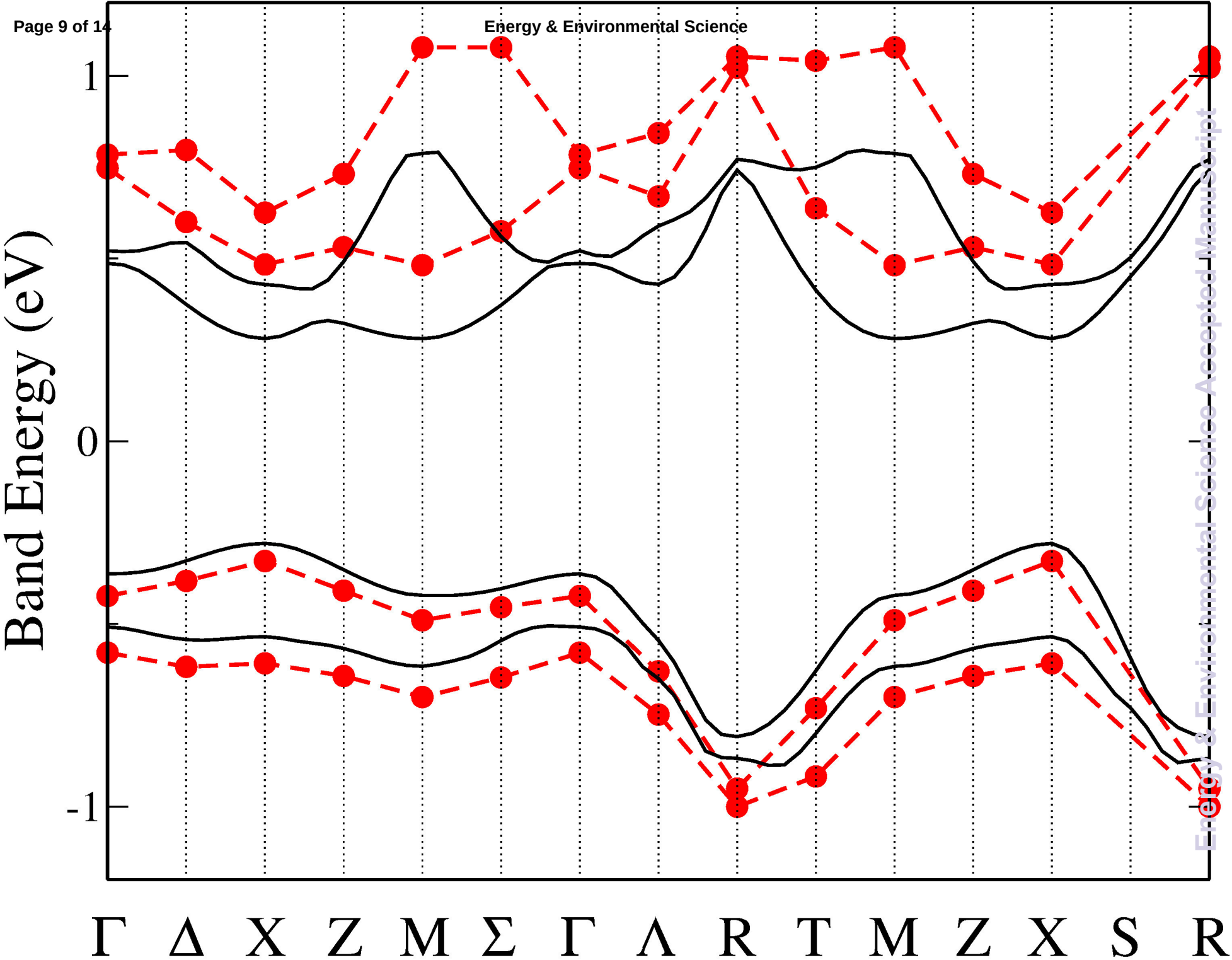

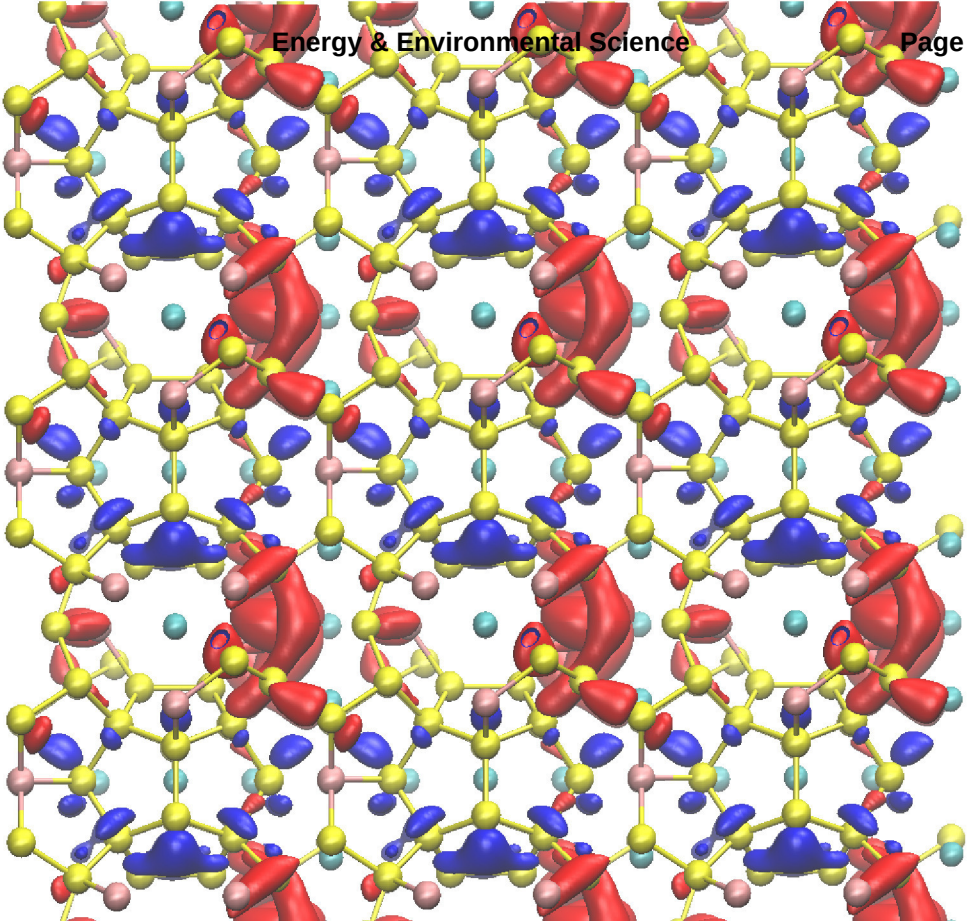

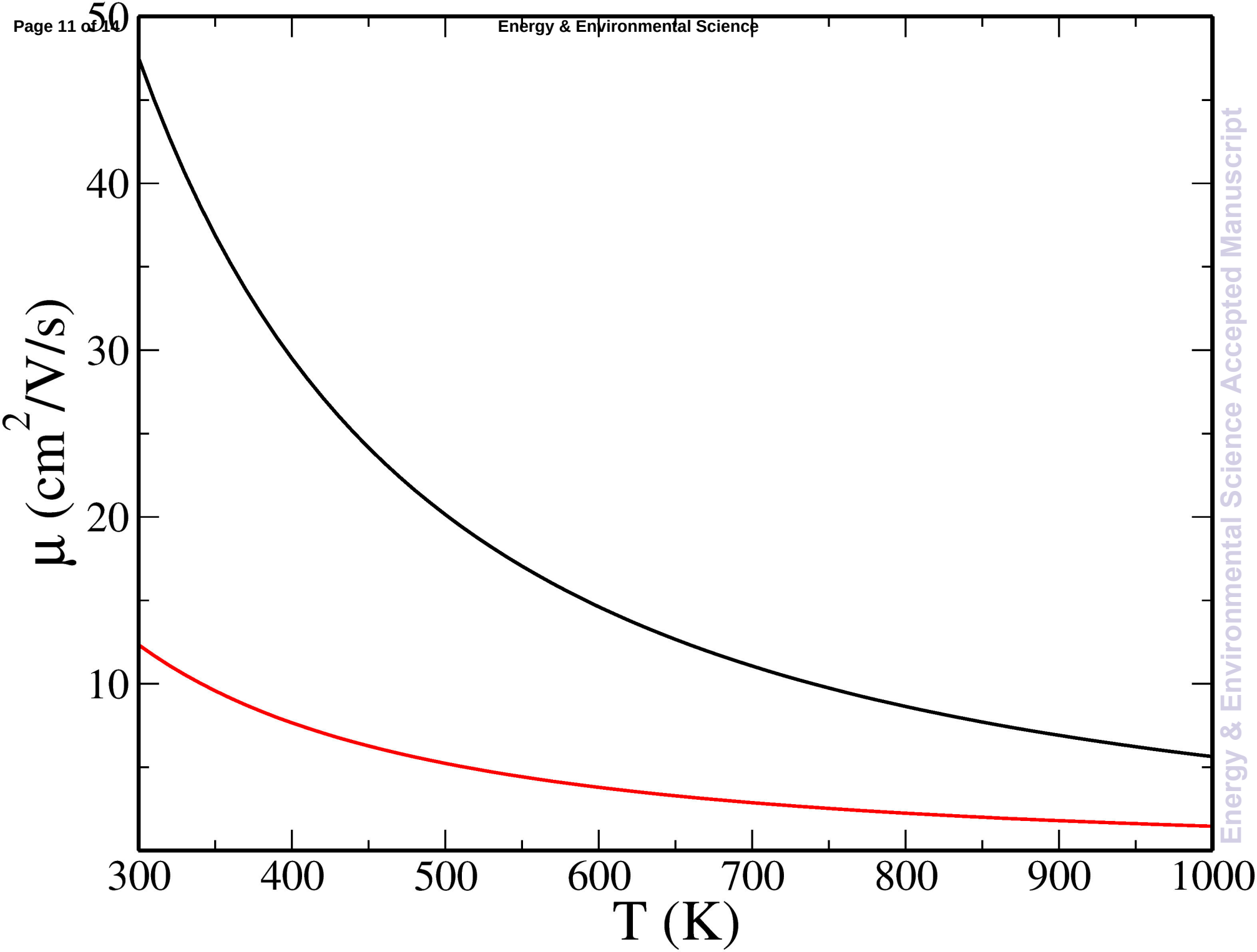

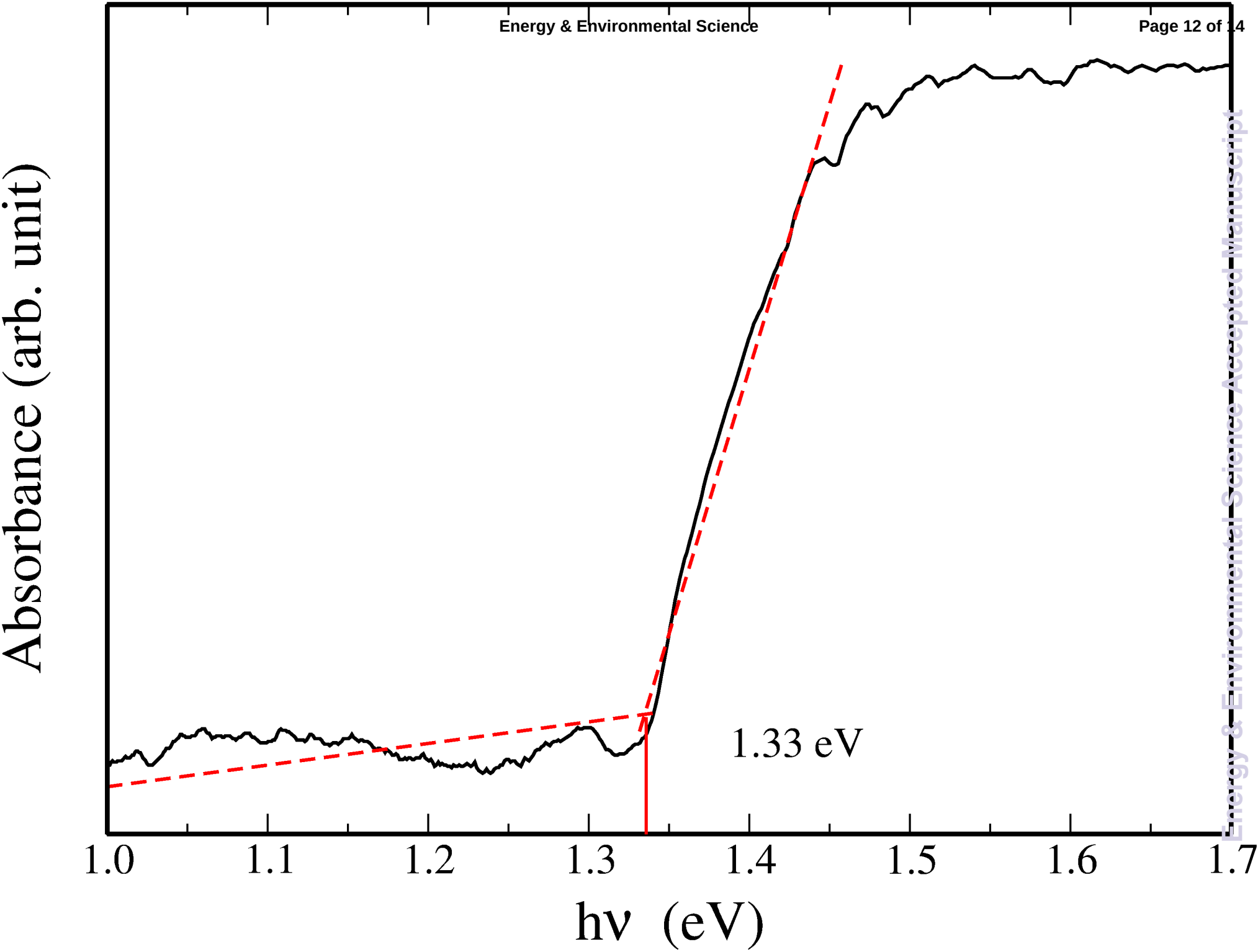

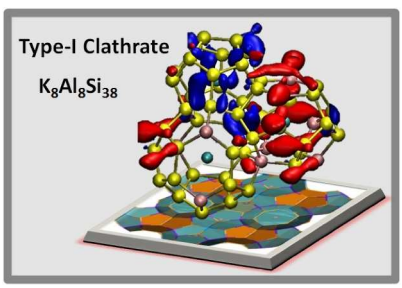

Manuscript title : Si-Based Earth Abundant Clathrates for Solar Energy Conversion

Manuscript ID: EE-COM-01-2014-000256

Broader Context

The desired properties of materials for solar energy conversion encompass a direct band gap in an energy range that maximizes absorption of visible light, and hole and electron mobilities allowing for efficient charge extraction, following light absorption. We show that the type-I clathrate $K_8Al_8Si_{38}$, composed of cheap, Earth abundant elements, is a promising materials for solar energy conversion, with a quasi-direct band gap of ~ 1 eV and mobilities much superior to those of amorphous silicon, a system already in use in solar cell devices.